Quantitative estimate of fracture density variations in the Nordegg with azimuthal AVO and curvature: A case study

LEE HUNT, SCOTT REYNOLDS, TYSON BROWN, and SCOTT HADLEY, Fairborne Energy
JON DOWNTON, CGGVeritas
SATINDER CHOPRA, Arcis Corporation

We investigated the accuracy of surface seismic attributes in predicting fracture density variations within the Nordegg Formation in west central Alberta. We know from core, drill samples, well-log, and drilling data that the Nordegg zone is fractured to some degree. These fractures are of interest because the reservoir has very low permeability, and therefore natural fractures may materially affect well performance. 3D surface seismic techniques such as amplitude variation with azimuth or azimuthal AVO (AVAz), variation of velocity with azimuth (VVAz), curvature, and coherence techniques are all tools that have been used to predict fractures in a qualitative fashion. In this study, we wanted to understand how well these attributes predicted the reservoir quality in a quantitative fashion. Previous quantitative studies have used image log orientation data or estimated ultimate recoveries (EUR) in vertical wells as validation data. The conclusiveness of these studies has been subject to several problems: firstly, the limited sample statistics provided by vertical wells applied to the validation of lateral variations, and secondly by the potential nonuniqueness of the EUR to fracture density relationship.

Our approach to the fracture prediction problem will add to these earlier attempts primarily by using the larger sample statistic provided by well-log data recorded in horizontal wells. Our validating data include fracture density data measured from a formation microimager log (image log) recorded in two horizontal wells as well as microseismic event data recorded over one of the two wells. Analysis of the image log data illustrates that the fractures are almost uniformly vertical and aligned, which satisfies key theoretical requirements of AVAz and VVAz. We also show that the surface seismic attributes share some similarities with the image log in their statistical behavior, particularly in the image log fracture density histogram and the histograms of AVAz anisotropic gradient, VVAz velocity difference, and most positive curvature attributes. We also demonstrate that image log fracture density correlates with these same surface attributes. Correlations between the surface seismic attributes and the microseismic event moments are also shown to be statistically significant. This statistical meaningfulness is mitigated by a concerning amount of scatter in all fracture predictions. The error in our predictions requires us to consider the possible breakdown in the predictive ability of the individual attributes, and points us to the potential advantage of using the surface seismic attributes together in either multilinear solutions or crossplotting procedures.

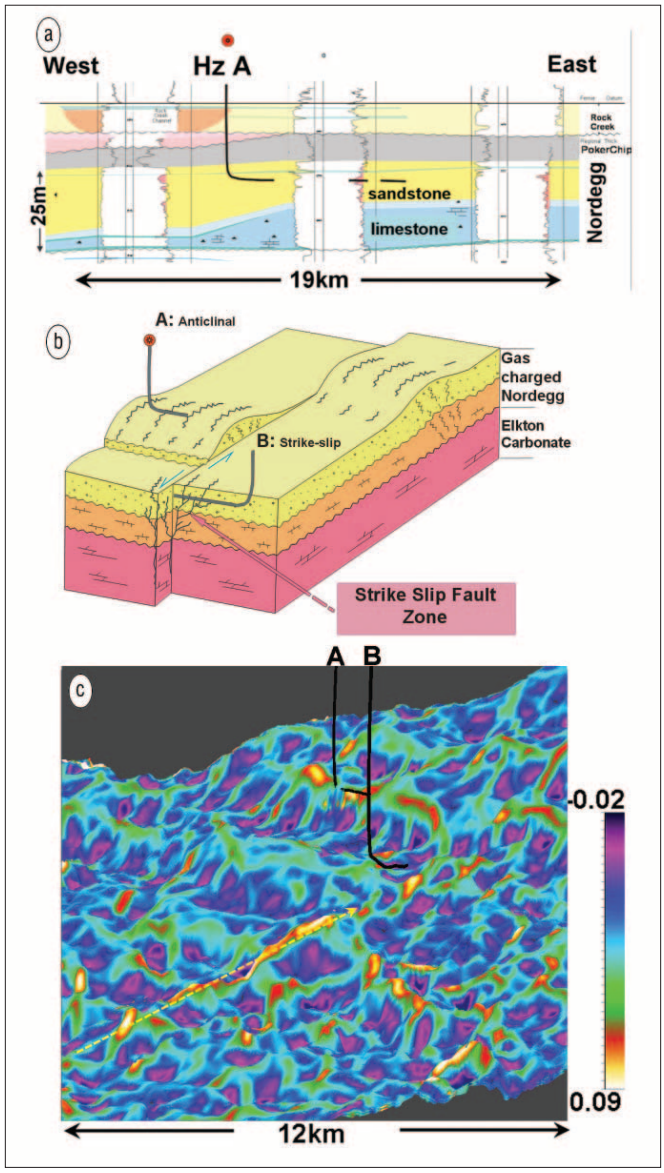

Figure 1. *Depiction of wells A and B. (a) Illustrates a stratigraphic cross section of the Nordegg in local wells. Log displays include gamma ray, and density porosity curves. The horizontal well A is depicted as if it intersects a nearby vertical well. (b) Schematic illustrating the relative position and setting of horizontal wells A and B. (c) A most positive curvature map of the Nordegg illustrated in a time relief map. The strike slip zone is indicated by the yellow arrow.*

The Nordegg Formation

The Nordegg Formation in the Columbia-Harlech area is typically a lower chert/carbonate rock type overlain by an upper porous quartz-arenite sandstone reservoir which is unconformably overlain by the Poker Chip shale. Porosity within the lower Nordegg is bio-moldic in origin and is developed from the remnant bivalves shells, pelecypods, and pelloids

deposited in the platform environment. The upper Nordegg contains a porous phosphatic sublithic arenite sandstone facies, which is interpreted as having been deposited in a shallow marine ramp setting. The intergranular porosity, within these meter-scale phosphatic sublithic arenite sandstone interbeds, was preserved due to the presence of silica and calcite cements during burial and compaction. Postburial migration of fluids partially-to-extensively removed the calcite cement and unstable grains (e.g., phosphate pellets) from the sandstone, establishing the reservoir-quality intergranular porosity and enhanced secondary porosity. Reservoir parameters of the Nordegg interval within the Columbia-Harlech area averages about 12 m of net pay (> 6% sandstone matrix porosity) with an average log porosity of 7% and 14% water saturation. The Nordegg is gas-charged. Core permeability ranges from 0.01–0.1 mD. The majority of the deliverability and enhanced permeability within the Nordegg is interpreted to come from the area's complex system of faults and fractures associated with regional strike-slip style faulting. Figure 1a illustrates the Nordegg reservoir in cross section.

There is extensive 3D surface seismic coverage in the area which enabled identification and mapping of the Nordegg's major structural features. Two wells (A and B) were drilled into several of the interpreted structural archetypes in the area. Figure 1b illustrates these structural archetypes and the relative positions of the wells. Well A was drilled along the strike of a folded anticlinal feature, and well B into a major strike slip feature. Figure 1c shows the exact positions of the wells on the seismic data with a most positive curvature attribute. All wells were drilled along strikes perpendicular to the regional tectonic interpretation of the maximum horizontal stress (σ_{hmax}). This was done so that fracture stimulations of the wells would be oriented to apply maximum stress in the same azimuth as σ_{hmax}. Image logs were acquired for wells A and B. A microseismic experiment was also performed during the completion of well A. Subsequent to drilling these wells, the 3D seismic data were processed in an attempt to produce attributes that characterize, explain, and predict the fracture density at the wells and throughout the rest of the 3D survey.

Previous studies

Most past attempts at objectively testing fracture prediction such as Lynn et al. (1999), Gray et al. (2003), Roth et al. (2009), and Khromova and Link (2010) used production EUR data from vertical wells to validate the attributes. The EUR of wells can be affected by other variables such as lateral boundaries, variable pressures, matrix permeability variations, variations in the completion of the well, and the drilling history of the field. These other related variables could act to limit or compromise our confidence in the EUR to fracture relationship. A more direct measure of fracture density and orientation, such as the fracture data produced by image logs, would be a desirable addition to the study of fractures. Image log orientation data have been used to tie estimated fracture orientations in vertical wells (Mazumdar et al., 2008; Roende et al., 2008). Boerner et al. (2004) related vertical well image log and other data with a seismic-based fracture density model, but the small number of wells and validation data formed a very small sample statistic. The image log data from a limited set of vertical wells have yet to form a sufficient sample statistic to conclusively study the variation in fracture density. Horizontal wells can be drilled long distances (greater than 1000 m) within a formation, which can enable the acquisition of a larger set of measured fracture density variations. The image log data (from horizontal wells) that we use should be a superior data element for testing fracture prediction, as the expected relationship to the seismic attributes is direct and measured over a large area within the formation. A comparison of the fracture predictors (AVAz, VVAz, curvature, coherence) against direct image log fracture density measurements will provide a clear, controlled, scientific basis for analysis. Microseismic event moments are used as a second, although less direct, element of validating data. The microseismic data cover an area of about 40 hectares, which comprises a significant region within which fracture density variations may be compared.

Theoretical background

AVAz describes the change in AVO as azimuth varies, while VVAz describes the change in velocity as azimuth varies. Both techniques can provide a direct estimation of relative fracture density and orientation if the fractures meet stringent physical criteria (Gray and Todorovic-Marinic, 2004). AVAz may be characterized by the near-offset Rüger (1996) equation:

$$R(\theta,\phi) = A + [B_{iso} + B_{ani}cos^2(\phi - \phi_{sym})]\sin^2\theta. \quad (1)$$

The equation models the reflectivity R as a function of azimuth ϕ for narrow angles of incidence θ, for an isotropic half-space over a horizontally transverse isotropic (HTI) anisotropic half-space. The HTI requirement means there must be a single dominant collection of near-vertical fractures. VVAz has the same physical requirements, as do the most commonly used forms of multicomponent seismic data fracture analysis methods. The equation is parameterized in terms of the P-wave impedance reflectivity, A, the isotropic gradient, B_{iso}, the anisotropic gradient, B_{ani} , and the symmetry axis of the horizontally transverse isotropic (HTI) anisotropic media, ϕ_{sym}. The anisotropy gradient is related to the fracture density as discussed by Lynn et al. (1996).

The 3D survey used in this study has a 660-m source line interval, 600-m receiver line interval and is 27 fold at the target. The acquisition geometry is typical for the area and target. These data will not produce adequately sampled, azimuthally sectored, and offset-sorted gathers, which presents a problem since the Rüger equation requires gathers sorted in limited offset and azimuth volumes. Gardner and Canning (1994) showed that sparse sampling would create artifacts in prestack migrated data. Their work did not consider the further damage that azimuthal sectoring would produce in the image gathers. Hunt et al. (2008) showed that five-dimensional interpolation (Sacchi and Liu 2005; Trad 2007, 2009) can infill missing offset and azimuths and reduce these

artifacts for AVO analysis. Gray and Wang (2009) used a physical modeling study to demonstrate that the interpolation, in addition to area weighting and bin borrowing (Zheng et al., 2001), generates AVAz estimates with greater accuracy and fewer artifacts. We employed all these techniques in the azimuthally sectored migration to produce AVAz results with the best accuracy. The VVAz anisotropy attribute was produced on the same imaged gathers in a horizon-consistent fashion. The Nordegg was one of the horizons used in the VVAz analysis. Chosen horizons were separated by about 50 ms. The VVAz anisotropy attribute is the percentage difference between the fast and slow azimuthal velocities within the Nordegg horizon interval.

Curvature attributes primarily describe the structural shape of the seismic data. Anticlinal features, especially hinge zones, may be clearly defined by most positive curvature maps.

Nelson (2001) describes how the points of greatest curvature relate to the points of greatest strain in the rock. The connection between curvature and strain is key to the validity of curvature fracture inferences. The most-positive curvature attribute may identify hinge zones on folds. Other causal variables of fractures such as lithology and in-situ conditions such as depth and pore pressure require that curvature measures be calibrated carefully for each horizon and area. Similarity attributes such as semblance or coherence are also commonly used to predict stratigraphic or structural breaks (including faults) in seismic data, and require calibration to well control for the same reasons as the curvature attributes.

The image log is a high-resolution borehole tool that can image fractures in the wellbore at the centimeter and millimeter scale. The image log tool provides its electrical image from micro-resistivity measurements. Luthi and Souhaite (1990) describe how these images are interpreted to reveal information regarding structure, sedimentary features, and rock texture. Fracture orientation, aperture, porosity, and density can also be determined from this log and were used in this study.

Microseismic experiments are sometimes used to observe and map hydraulic fracture stimulations of reservoirs. Seismic events (moments) observed around the time of stimulation are presumed to be related to fracture growth. Therefore, new fractures may be mapped and calibrated from the seismic (event) moments as observed from surface or subsurface microseismic monitoring during and after stimulation. Maxwell et al. (2009) observed that the microseismic events result from an interaction between the stresses induced upon the formation during stimulation, the preexisting stress regime within the rock, and pre-existing fractures. As a result, there should be a correlation between microseismic events and preexisting fractures. Bayuk et al. (2009) suggested that certain microseismic events followed the orientation of known natural fractures and signified deformation within them. Their work suggested a sharing of microseismic events along the direction of the hydraulic fracture treatment where new cracks formed, and the preexisting natural fracture network, oriented with different azimuths. The observations imply the microseismic events are not necessarily only correlated to the natural fracture system, but may also be affected by the particular stress field created by the hydraulic fracture stimulation. This stress field may or may not be in the same direction as the natural fracture system, and suggests a complex interplay between paleo-fractures, present-day stresses and the stress imparted to the formation under fracture stimulation. The multiple causes of microseismic events require some

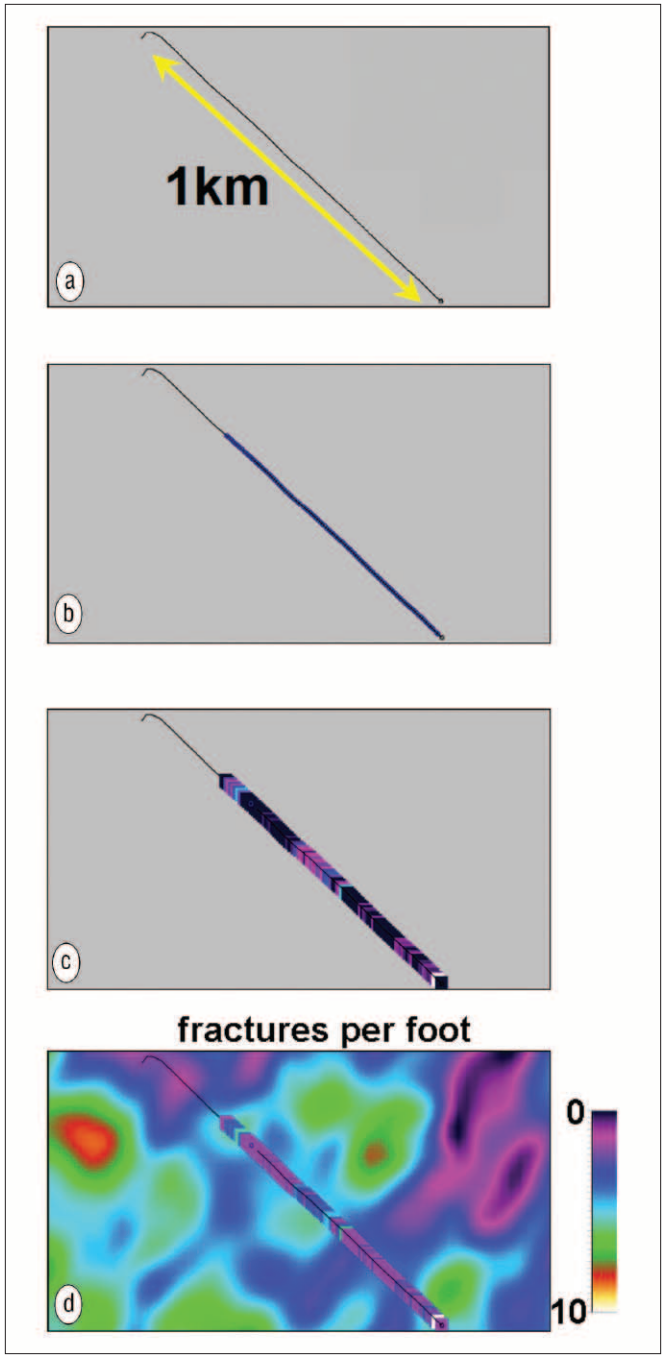

Figure 2. *The extraction of fracture estimates from the image log and the seismic data at well B. (a) The path of horizontal well B. (b) Well B with the vertical wells created as image log data bins. (c) The bins with image log fracture density values in fractures per foot. Brighter colors represent higher values of fracture density. (d) The image log density in fractures per foot located over a gridded 3D attribute (the attribute is a linearly weighted combination of AVAz crack density and curvature, similar to Figure 7d).*

caution and interpretation in their use as a validation tool for surface seismic fracture attributes. In this study, the wells were drilled so the fracture stimulations would be oriented to apply maximum stress in the same azimuth as σ_{hmax}. This may reduce the complexity in the microseismic event behavior, and increase the expected correlation between microseismic events and the natural fracture system. Despite the complexities and potential nonuniqueness of the microseismic events to the natural fracture relationship, the use of microseismic data has advantages over other validation data. The microseismic event data generally form a large spatial sample statistic. There are commonly hundreds of microseismic events, and instead of following a well path, they are distributed spatially about the well. The support size and location accuracy of the microseismic is also much closer to typical seismic bin sizes. This is in stark contrast to any borehole logging information, which is recorded with subseismic support and investigates only a few inches or a few feet into the formation.

Data and methodology

The 3D surface seismic data (3D) used to produce the seismic attributes is the same 3D discussed in Hunt et al.'s (2008) interpolation and AVO case study. The same interpolated data were migrated in azimuthal sectors to produce data for AVAz and VVAz attribute estimation. Volumetric curvature and coherence attributes were produced from specially processed and conditioned migrated stacks at high and low resolutions by methods described by Chopra and Marfurt (2007). Attribute values were extracted from each of these processed volumes at the Nordegg level and were gridded in a consistent manner for each volume. The VVAz anisotropy attribute was determined by extracting an interval anisotropy value from the data volume just below the top of the Nordegg pick. The most-positive curvature attribute and coherence attributes were extracted in the same fashion. The AVAz attribute was calculated using a larger window of the Nordegg and calculating the rms average of the anisotropic gradient within the window. The AVAz attribute was not sensitive to the window size, provided an rms average was used. This insensitivity may suggest the average fracture densities in the sandstone and limestone facies of the Nordegg were not significantly different.

In order to test whether the seismic attributes predict fractures in the Nordegg, we need to extract the image log data with the 3D data at the same locations. This presents challenges regarding scale and support. The image log data are recorded with resolution on the centimeter and millimeter scale, and are sampled with average values at a fraction of a meter. The bins from which the 3D attributes are extracted are 30 × 60 m. In order to bring these data together, we created a new binning scheme for the image log data, where we created image log data bins every 10 m along the horizontal wellbore paths. Image log data were averaged within the bins. This averaging brings the support size of the image log data closer to that of the seismic, although we kept the bin size small enough to allow us to consider further averaging later. Each image log data bin was dubbed as a pseudo-vertical well

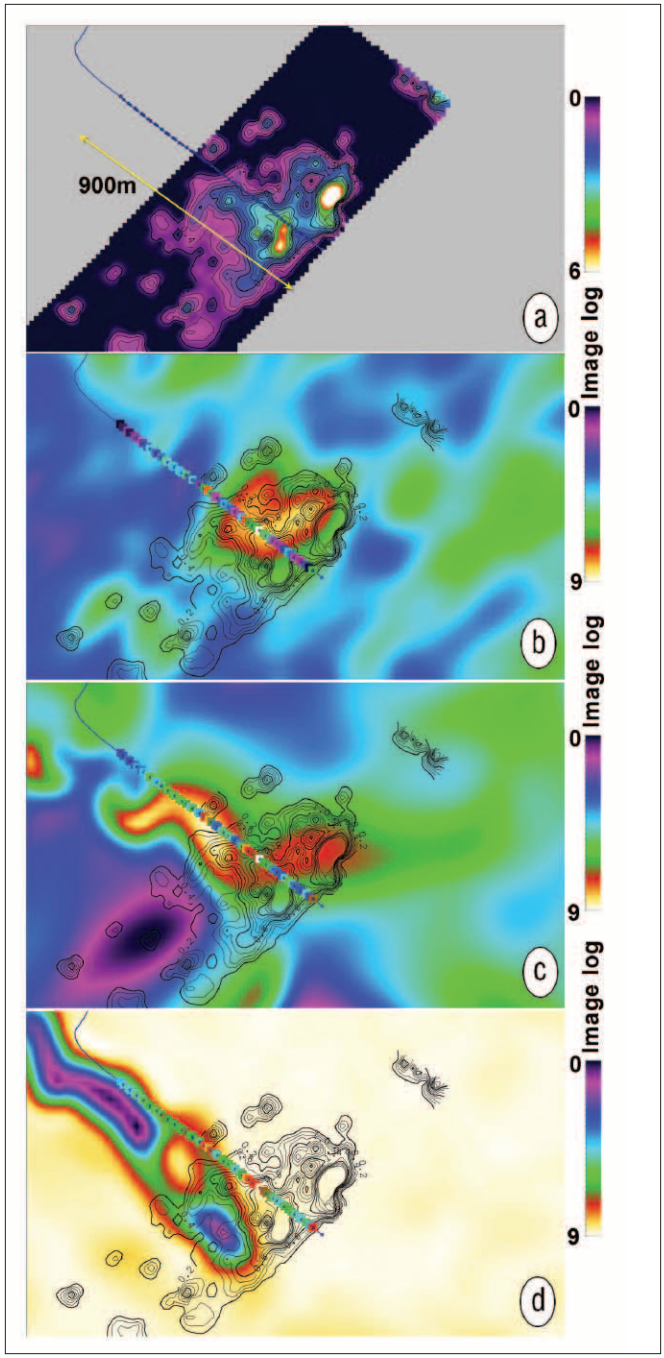

Figure 3. *The microseismic and the surface seismic at well A. (a) The microseismic cumulative event moments. (b) The contoured event moment data overlain upon AVAz crack density data. (c) The same comparison for low-resolution most-positive curvature data and the microseismic moment data contours. (d) The same comparison for coherence. In all cases, brighter (yellow) colors represent higher values. The image log data are fracture density in fractures per foot.*

with the image log fracture density given as a formation top value. Image log and gridded 3D attribute data could then be extracted together at each of the dummy well locations and exported as ASCII data for analysis. Figure 2 illustrates this element of the procedure. Both wells A and B were drilled along the same azimuth, which is perpendicular to σ_{hmax}. This orientation could introduce a bias towards encountering fractures oriented in the direction of σ_{hmax}.

The microseismic events must be extracted with the surface seismic attributes so they can be correlated. Events from four different completion stages were summed into one microseismic event moment horizon that we could locate and bin within the 3D volume. Microseismic events were detected further than 400 m away from the horizontal well bore. Bins with no events were given a moment value of zero. These events could also have been given small values corresponding to the limits of detection of the experiment. Either approach has a degree of arbitrariness and has a similar effect on the comparisons carried out later. Correlations with surface seismic attributes were carried out by extracting the microseismic horizon data and the 3D attribute data at the same bin locations. This extraction was limited to an area that represented an envelope of the observed microseismic events, in order to maintain the meaningfulness of the no-event data. There were 196 surface seismic bins within the extraction area, and 124 of those bins had microseismic event moments within the range of detection. Figure 3 illustrates this element of the procedure. The microseismic cumulative moment is displayed in Figure 3a. Figures 3b and 3c illustrate the AVAz and most positive curvature attributes with the microseismic cumulative moments displayed as a contour overlay. These displays show a possible relationship between the microseismic data and both surface seismic attributes. In a qualitative sense, both attributes appear to have regions of similarity and dissimilarity to the microseismic data. Figure 3d makes the same comparison for the coherence attribute, but does not illustrate an obvious qualitative relationship between coherence and the microseismic data.

Image log data: Do we have an HTI media?

The image log data from wells A and B represent combined log information from 1800 m of Nordegg reservoir. Figure 4 describes the statistical behavior of the image log fracture density data. These data very clearly show that the fractures are overwhelmingly vertical, have a common azimuth, and obey a power law distribution. The two sets of azimuths with respect to north shown in Figure 4b are actually the same azimuth; i.e., they are 180° apart. The image log data suggest that the fractures might induce HTI anisotropy, which is assumed by both our AVAz and VVAz methods.

Attribute data: similar to the image log data?

The distributions of the surface seismic attributes should have similar characteristics to the image log data if they are to estimate fracture density. Figure 5 illustrates the distributions of our key surface seismic attributes. The estimated azimuth data shown in Figure 5b are remarkably similar to the image log data. The AVAz anisotropy, VVAz anisotropy, and curvature attribute histograms are not as well matched to the image log fracture density. Although these histograms are asymmetric in the same sense as the image log data, they less clearly follow power law behavior. These attributes may also illustrate a second population in the data as shown in Figures 5a, 5c, and 5d. This second population could be a result of the difference in the scale of observation of the surface seismic

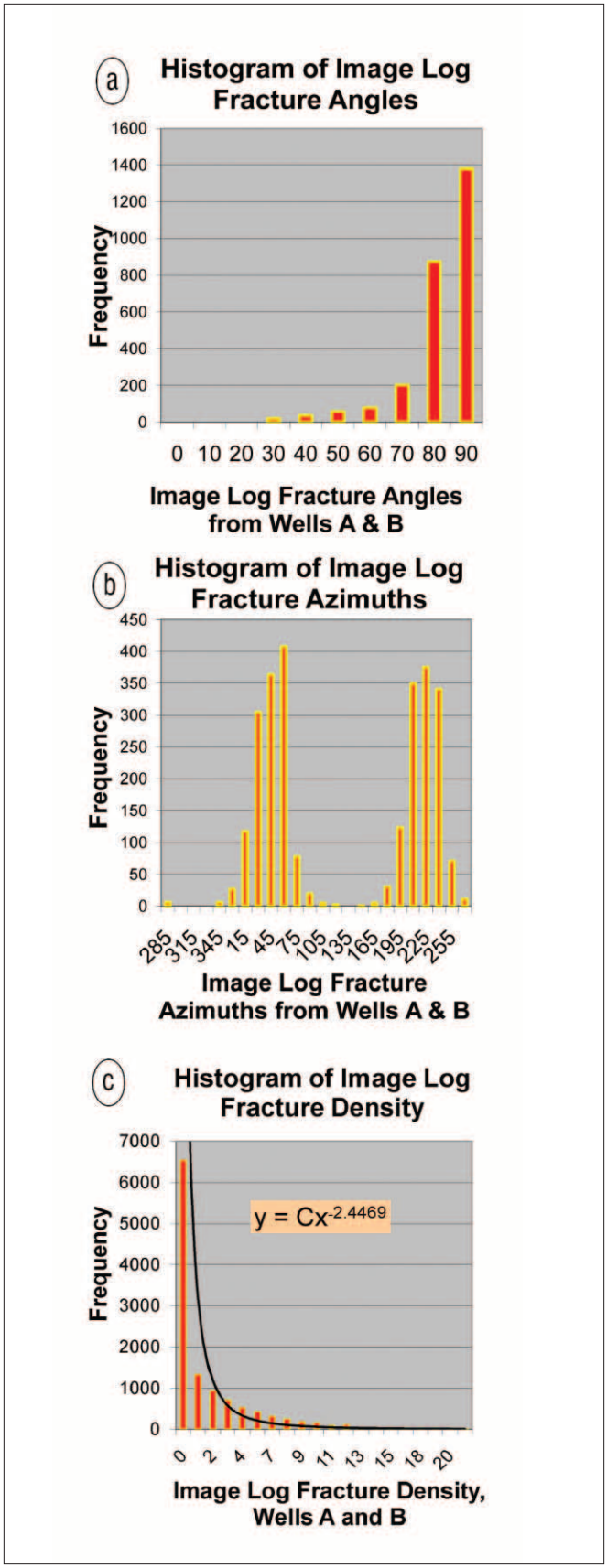

Figure 4. *The statistical behavior of the fractures observed by the image log. (a) The angle from the horizontal. 85% of the fractures had an angle of 80 °or more. (b) The azimuth from north. (c) The density distribution in fractures per foot.*

attributes and the image log data. The second population might also be telling us something important about the fractures. Nelson (2001) describes type I and type II fractures on fold systems. The type I fractures should be oriented in the direction of σ_{hmax}, and should be widely distributed, while the type II fractures will follow the strike of the fold and be most dense in the hinge zone. The points of maximum curvature will represent the hinge zone, and could be a location where both fracture types exist in abundance. The highest curvature values all occur on the hinge of the fold along which well A is drilled.

Correlation coefficient	AVAZ (B ani) RMS	VVAz Velocity anisotropy	Curvature Maximum	Curvature Low resolution most positive	Coherence Energy ratio
Raw image log	0.484	0.426	0.602	0.510	0.175
Averaged image log	0.612	0.539	0.739	0.628	–0.215
Averaged image log, low curvature population	0.742	0.541	0.676	0.355	0.184

Table 1. *Correlation coefficient summary for the 3D attributes regressed against the image log fracture density data.*

P Values (61 points)	AVAZ (B ani) RMS	VVAz Velocity anisotropy	Curvature Maximum	Curvature Low resolution most positive	Coherence Energy ratio
Averaged image log	1.1E-06	2.5E-06	4.0E-12	4.4E-09	9.8E-02
Averaged image log, low curvature population	1.4E-08	3.6E-05	1.0E-07	5.0E-03	5.8E-01

Table 2. *summary of P-values calculated for the regressions summarized in Table I. Lower P-values imply higher confidence that the correlation is not caused by chance. P-values higher than 0.01 = brown.*

It is possible the HTI media description of the rock will fail where both fracture sets exist, depending whether one fracture type is dominant over the other and how that dominance may change laterally, and at what lateral scale that change occurs. This could represent a local breakdown in AVAz and VVAz. The AVAz estimated azimuth distribution of Figure 5b is very similar to the image log fracture azimuth distribution of Figure 4b, with dominant fracture strike azimuths of about 50° east of north, and is the orientation we expect the type I fractures to have. This is the expected orientation for σ_{hmax}, and is perpendicular to the well path. This orientation information shows little evidence of type II fractures. This could mean: firstly, there are not many type II fractures in the area, or secondly, the wellbore orientation is biased against encountering the type II fractures, or thirdly, that the type II fractures may still exist very near the wellbore.

This third possibility also points to potential issues consequent to scale differences: the seismic bins collect data on a 30 × 60 m rectangle, while the wellbore is only a few inches in diameter regardless of how we average the data in the length dimension. These scale differences plus the uniform azimuth of our well paths do not allow us to be conclusive on this point.

Image log data correlations with surface seismic attributes

3D attributes were extracted at the image log data bins along the horizontal trajectories of

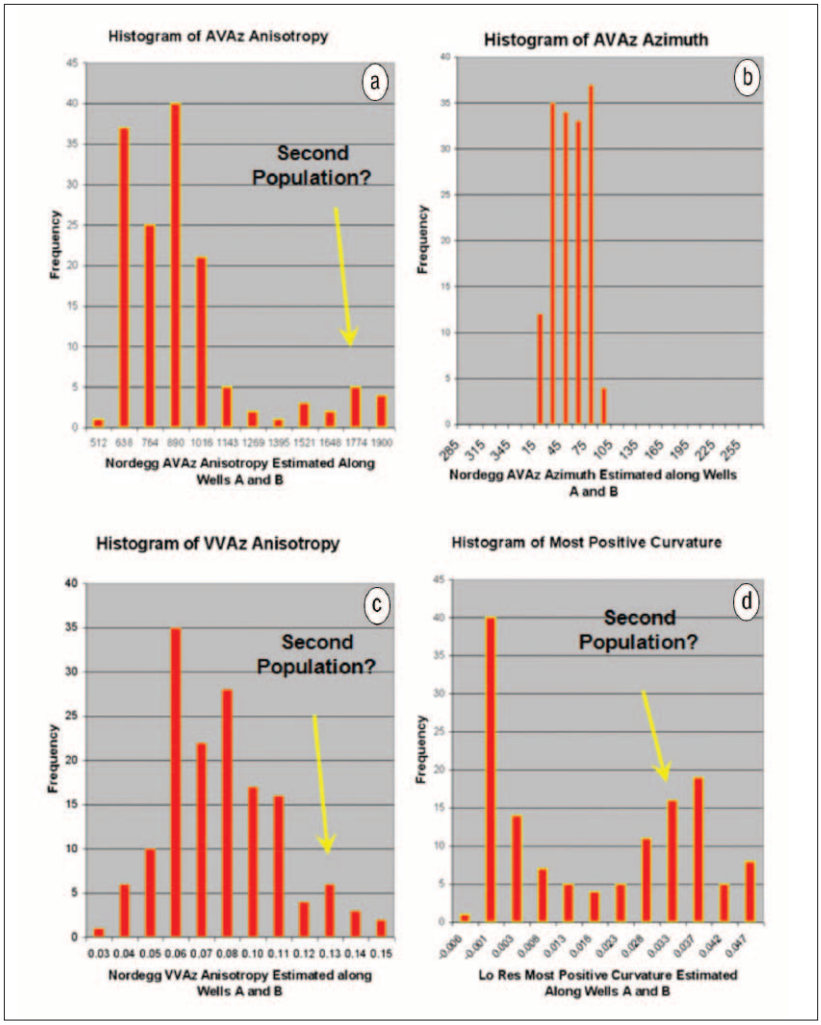

Figure 5. *The frequency distributions of the surface seismic fracture predicting attributes. (a) AVAz crack density. (b) AVAz azimuth. (c) VVAz anisotropy. (d) Low-resolution most-positive curvature.*

Correlation coefficient	Microseismic cumulative moment (# of data points)			
	All data (196)	All data, 1 cull (195)	No null events (124)	No null events, 1 cull (123)
AVAz (B ani) RMS	0.567	0.638	0.452	0.541
VVAz anisotrophy	0.257	0.310	0.214	0.290
Maximum curvature	0.284	0.353	0.194	0.285
Low resolution most positive curvature	0.294	0.370	0.092	0.166
Coherence	0.076	0.065	0.276	0.319

Table 3. *Correlation coefficient summary of the 3D attributes regressed against microseismic event moments.*

P-values	Microseismic cumulative moment (# of data points)			
	All data (196)	All data, 1 cull (195)	No null events (124)	No null events, 1 cull (123)
AVAz (B ani) RMS	4.7E-18	1.2E-23	1.4E-07	1.0E-10
VVAz anisotrophy	3.0E-03	1.1E-05	1.7E-02	1.1E-03
Maximum curvature	1.0E-04	4.3E-07	3.1E-02	1.4-03
Low resolution most positive curvature	2.9E-05	1.0E-07	3.1E-01	6.6E-02
Coherence	2.9E-01	3.7E-01	1.9E-03	3.0E-04

Table 4. *Summary of P-values calculated for the regressions summarized in Table 3. Lower P-values imply higher confidence that the correlation is not caused by chance. P-values higher than 0.01 = brown. Only the AVAz attribute passes the 1% significance level test for all populations.*

well A and well B. These data were correlated with the image log fracture density values in several ways, including a simple regression of seismic bins to image log bins and a regression where the image log bins were smoothed by a seven-point smoother to more closely approximate the seismic bin size.

Different smoothing schemes and smoother lengths were tested, all of which produced similar results. Another regression was produced where a potential second population within the attribute data was excluded. The second population was identified in Figure 5, and was thought to potentially be the result of a difference in the scale of observation, or even a breakdown in the attributes themselves at or near a hinge zone and area of multiple fracture sets. The anomalous population was separated in the same way for each attribute through a resorting of the data by curvature values. Only the AVAz attribute benefited from the separation of the high curvature population. Table 1 summarizes the correlation coefficients for these regressions. This table includes regressions from the original sampling of the image log data as well as the smoothed data and the population restricted data so that the entire analysis can be compared. The statistical significance of these correlation coefficients was also considered by calculating the P-values for each regression. Only the averaged image log data correlations were evaluated to ensure the correct number of samples were considered in the calculations. Table 2 summarizes the P-values, and identifies the 1% confidence level with brown highlighting. Only the coherence attribute failed the 1% test. This test suggests that the correlations of the AVAz, VVAz, and curvature attributes with the image log fracture density were statistically significant. Figure 6 illustrates several of the crossplots from which the correlation coefficients were calculated. The AVAz and curvature attributes had strong correlations, while the VVAz attribute had a correlation that was not as strong, but still statistically convincing. The coherence attributes did not show a meaningful data correlation; in fact, these correlations were either low in the comparison to image log average, or nonphysical in the low curvature population.

These regressions can be used to predict fracture density from the seismic attributes. Figure 7 illustrates four such maps near well B. The coherence map of Figure 7c does not have an obvious relationship to the image log data in the well. There is little range in the coherence-based fracture density estimate at well B, due to the lack of coherence anomalies in the area of the well. The best map is found in Figure 7d, which employed a multilinear regression of AVAz and curvature attributes. This map uses the attributes in a complementary fashion. The scatter plot resulting from the multilinear regression is shown in Figure 8. Other combinations of attributes were tested in multilinear solutions, but the AVAz and most positive curvature attributes had the best correlation coefficient, which was 0.74. The addition of VVAz or coherence attributes did not improve the regression.

Microseismic event correlations with surface seismic attributes

The microseismic event moment data were regressed with the 3D attribute data binned at the same locations. This was done in four different ways: a simple regression utilizing all the data, a regression with a single outlier point culled, a regression with the null or nonevents culled, and a regression where both the null events and the outlier were culled. Each case had more than 120 sample points to be compared. Two crossplots from the regression work are shown in Figure

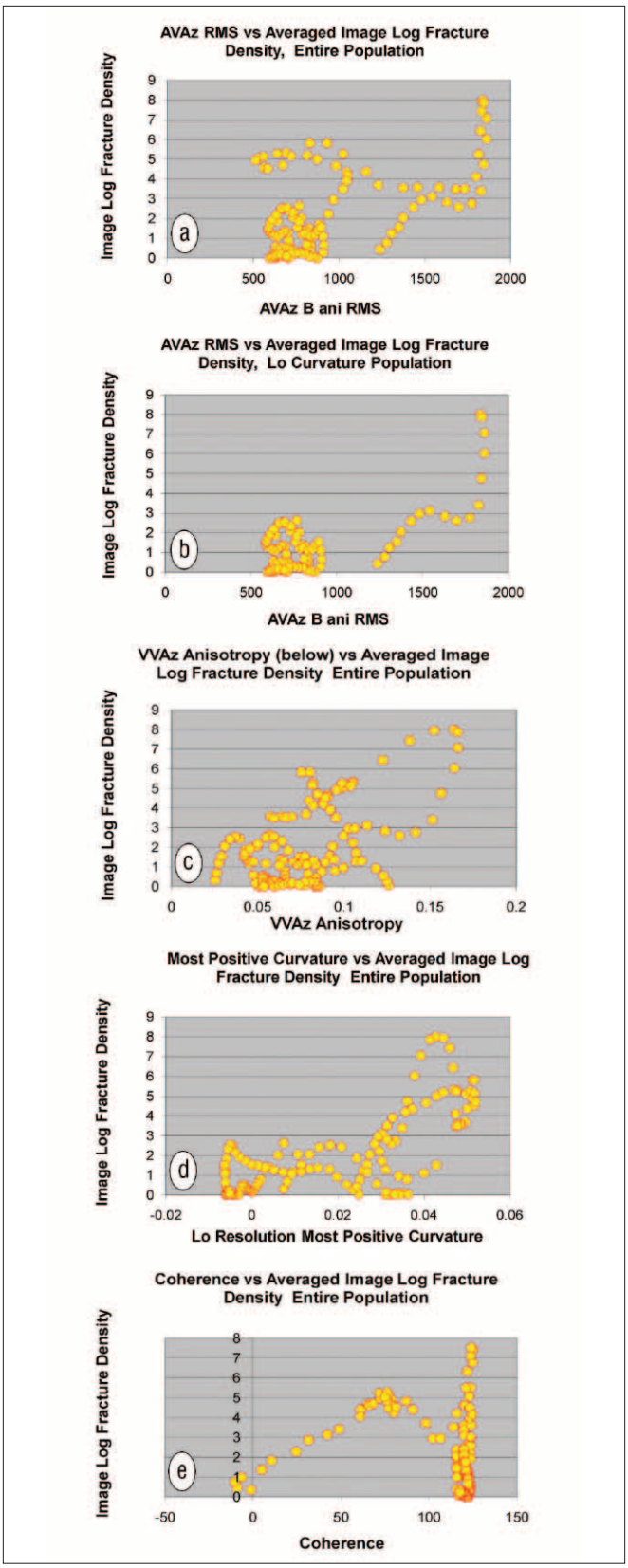

Figure 6. *The crossplots of image log fracture density and seismic attributes. (a) AVAz versus image log fracture density. (b) The same, except the high curvature population is not included. (c) VVAz versus image log fracture density. (d) The most-positive curvature versus image log fracture density. (e) Coherence image log fracture density.*

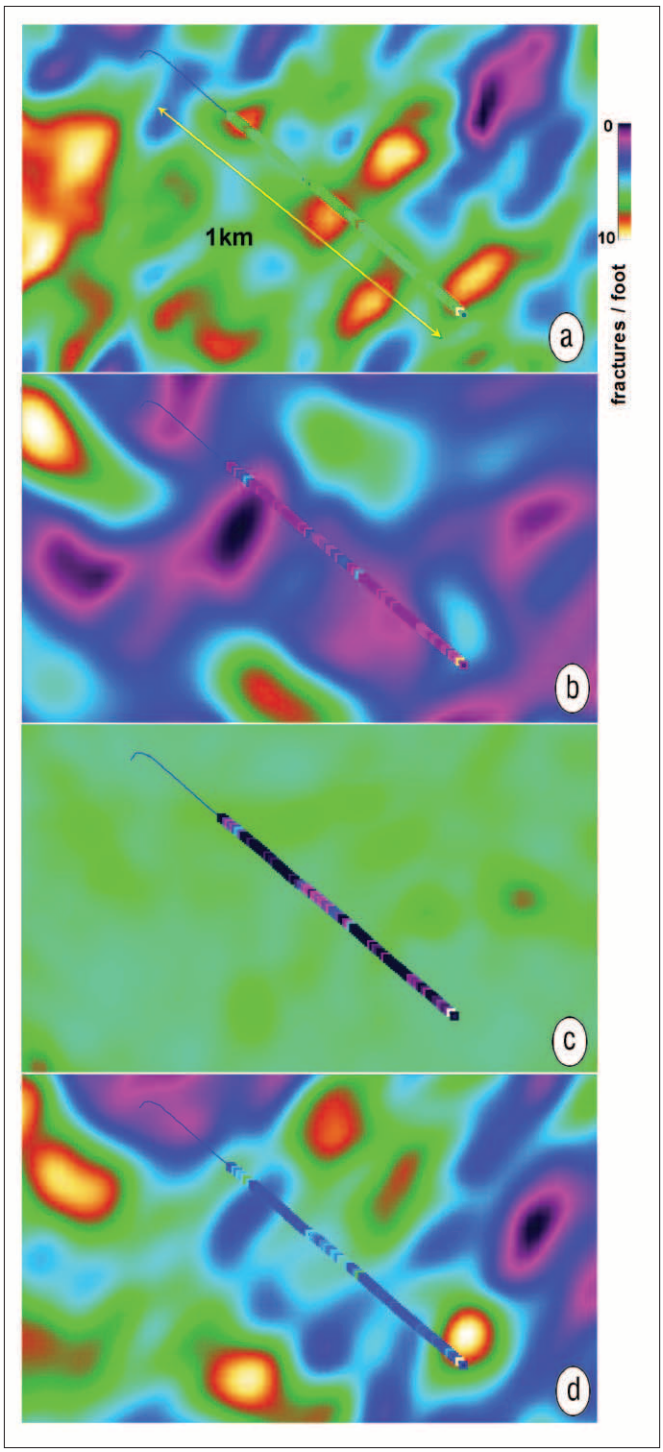

Figure 7. *Fracture density predictions from seismic data at well B. (a) The fracture density predicted from AVAz data. (b) The fracture density predicted from low-resolution most-positive curvature data. (c) The fracture density predicted from coherence. (d) The fracture density predicted from AVAz and curvature data. The image log data are fracture density in fractures per foot.*

9, on which the null or nonevents and the data outlier are identified. We present these observations cautiously since the absence of a microseismic event is clearly important information, but our handling of that information is less sure. Similar results would also be reached by alternatively making the

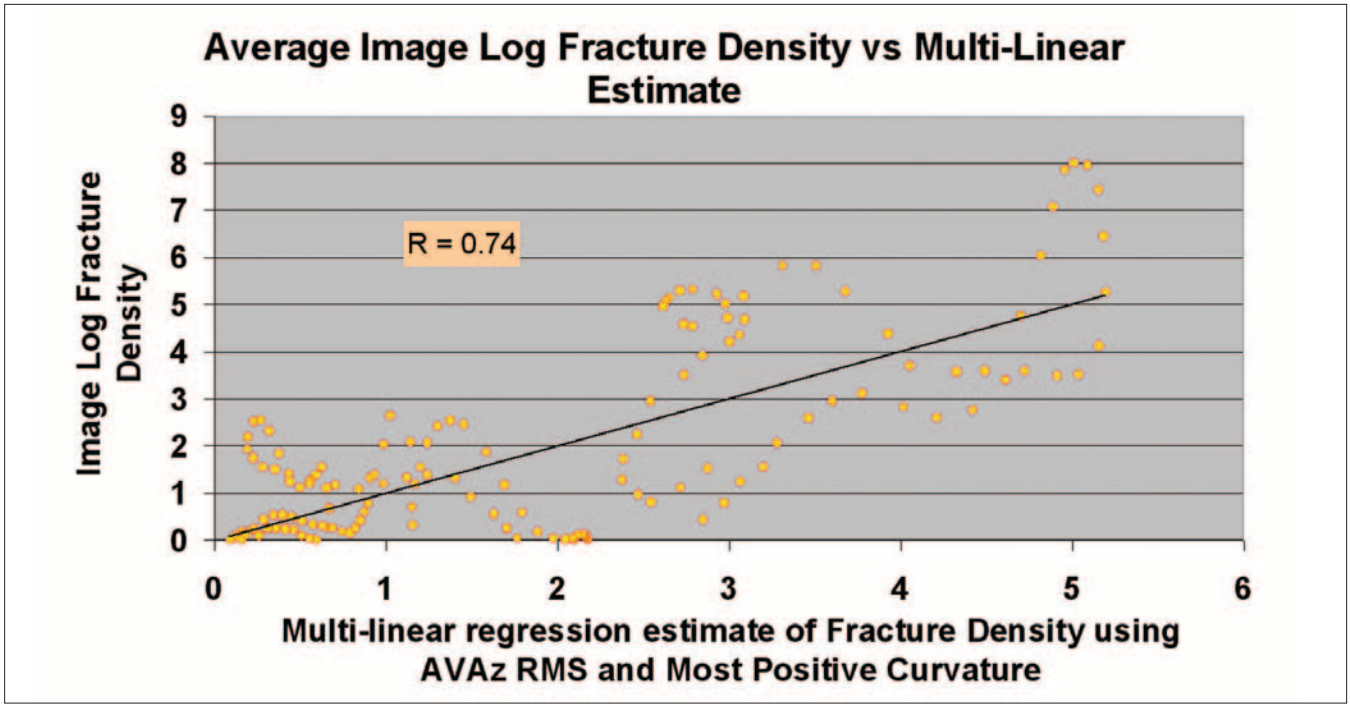

Figure 8. *Crossplot of image log fracture density versus a multilinear regression estimate of fracture density. The multilinear regression uses AVAz rms and most-positive curvature values. The correlation coefficient for this regression is 0.74 . All data were used in this scatter plot.*

nonevent data a small value corresponding to the limits of detection in the microseismic experiment. Either method has a degree of arbitrariness, so we opted to simply assign nonevents the value of zero. Figure 9b shows a strong correlation, which may fit better to an exponential curve. The high correlation between the microseismic and the AVAz attribute is consistent with the map displays of Figure 3. Table 3 summarizes the correlation coefficient values of those regressions. The AVAz attributes were clearly the best, followed by curvature and VVAz attributes. The statistical significance of these correlation coefficients was also considered by calculating the p-values for each regression. Table 4 summarizes the P-values for the regressions. Only the AVAz attribute passed the 1% test for significance for every variation in our population. Note that most high P-values occurred when we excluded the nonevent data. The coherence attribute was positively correlated to the event moment, which is counter to our expectation. Higher coherence is normally interpreted to mean fewer fractures or faulting, the opposite of this correlation. This likely means that the coherence correlation is spurious.

AVAz and most positive curvature: An advantageous combination

The multilinear regression of the AVAz and curvature attributes yielded a superior predictor of fractures. The notion of a potential breakdown in AVAz at or near hinge zones may suggest a reason why. All attributes suggested the possibility of a second population within the data, but only the AVAz attribute regression benefited from excluding data sampled at the very highest curvature values. Further validation data are required to better understand the significance of this potential second population. These high curvature values are likely

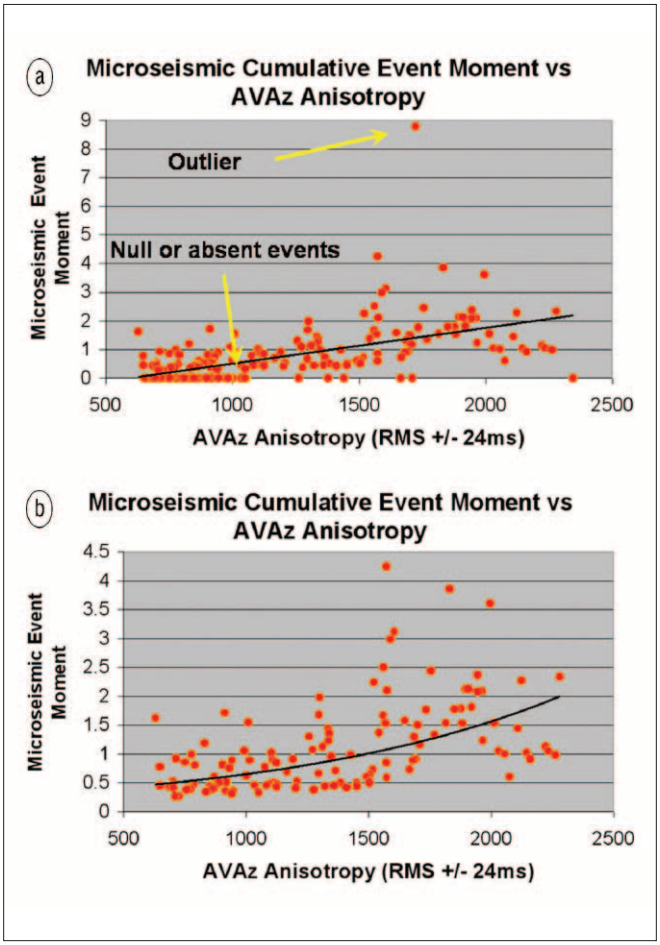

Figure 9. *Microseismic event moments crossplotted against an AVAz crack density attribute. (a) All data. (b) The null events and an outlier event culled.*

to be in the hinge zone, which is also where Nelson (2001) has suggested the greatest density of type II fractures may be present. As mentioned earlier, this may be where the HTI description of the rock loses validity. If the hinge zones may be an area of greatest uncertainty in some AVAz estimates, the addition of the robust curvature data may be complementary. Another method of combining AVAz and curvature is through crossplotting and facies mapping. Figure 10 illustrates such an effort. Figure 10a illustrates the crossplot of the most positive curvature and AVAz attribute. Strong values of curvature are given specific colors (light blue), while strong values of AVAz are given other colors (purple). Strong values of both are yellow. Figure 10b illustrates the facies map produced at well A from this color assignment. This map bears a startling resemblance to the microseismic cumulative moment map of Figure 3a.

Even with the multilinear regression or the crossplotting methods, the relationship between the image log fracture density and the predicting variables must be described as statistical. We do not dispute that this work shows a relationship between the attributes and fracture densities; however, the degree of scatter is concerning and should be considered further. The reasons for this scatter may include:

1) All the data we used, including image log, microseismic, and surface seismic, are soft data. Consequently, they have an element of interpretability; they each have measurement errors; and they measure at different scales.
2) The failure in validity of the attributes. AVAz could fail where there are multiple fracture sets. Curvature, an inference method, fails to account for other causes of fracture density variation such as changes in rigidity of the rock or bed thickness. Curvature may fail if stress in the rock is not observable as a measurable change in shape on the seismic (no prediction of strain).
3) Noise or other limitations in the seismic data. Migration noise may still be present in the AVAz and VVAz data. The data may not be sufficiently well sampled to properly represent the azimuthal variation even with interpolation.
4) The amount of scatter that each attribute might be expected to have is difficult to generalize because the reasons for the error are different for each predictor. Careful consideration of the potential causes for error should be made in every case. These limitations in our method must be recognized in forming realistic and practical strategies relative to fracture prediction. The use of multiple variables with overlapping or complementary areas of validity is one approach to consider in the early stages of fracture assessment. Future drilling in the Nordegg is being considered only along well paths where both the AVAz and curvature attributes predict fractures, such as was seen in most of well A's path.

Conclusions

These experiments illustrate that the AVAZ, VVAz, and curvature attributes correlate strongly with image log fracture density, and should be valid predictors of fractures in the Nordegg of this area. Similar observations were made using the microseismic data, a less direct validator of fracture prediction, also exhibited strong correlations. The large, spatially distributed sample size and similar support make microseismic events an intriguing data element to compare and cross-validate with surface seismic fracture predictors. The comparison of microseismic to surface seismic should be carried out with other data to determine if the results are repeatable. Further experiments may reveal how important the wellbore orientation and hydraulic fracture orientation were with reference to σ_{hmax} and the orientation of the preexisting natural fractures. This work indicated that AVAz was the best single predictor of fracture density, although curvature attributes were almost as good. We also observed that despite the predictive correlations, significant scatter remained in the data comparisons. That scatter likely has implications to our data quality as well as the theoretical limitations of our methods. In consideration of this, we attempted to use com-

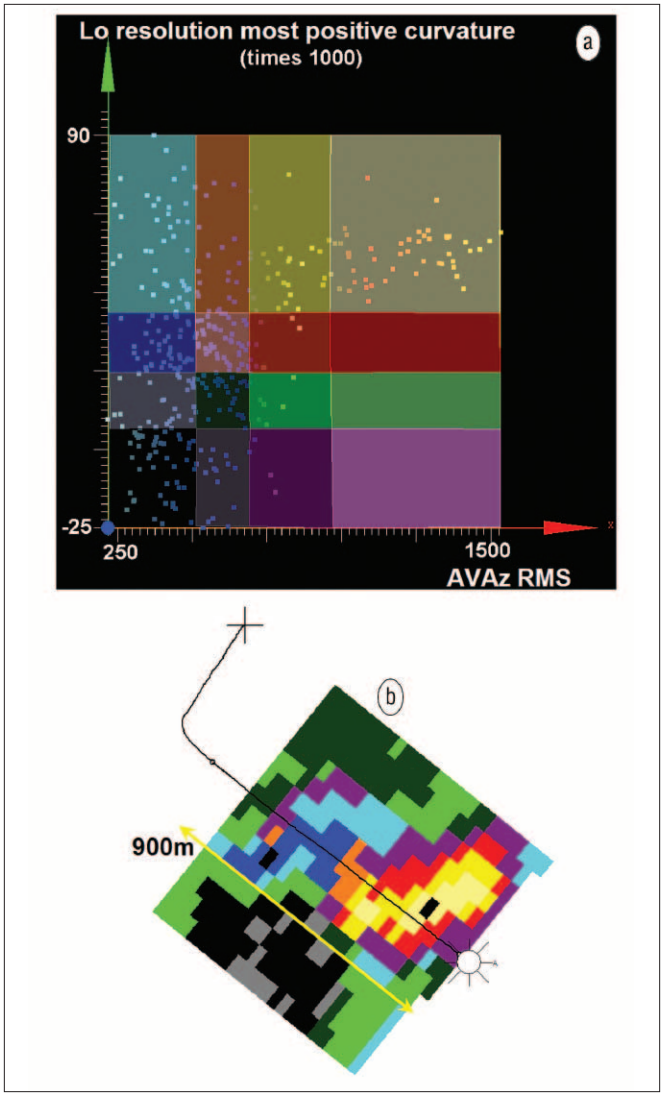

Figure 10. *Crossplot of AVAz rms and low-resolution most-positive curvature values at well A. The crossplot is divided so we can identify areas with high AVAz, high curvature, or both by color. (a) The crossplot. (b) The map that comes from it.*

binations of the attributes in multilinear and crossplotting approaches. These results were most accurate when AVAz and curvature were used together. The advantage of using these attributes together may lie in the areas of validity for each attribute: AVAz can directly detect fractures, but may fail in hinge zones where multiple fracture sets are most likely to exist, while the curvature attribute identifies the hinge zones, but may not infer the fractures that exist in less obviously deformed areas.

A surprising conclusion from this work was that the coherence attribute did not predict fracture density or microseismic event moments for the Nordegg in this area. For the kinds of fractures that exist in the Nordegg of this area, AVAz and curvature are a more useful combination than coherence and curvature, which have been used to advantage in other areas. TLE

References

Bayuk, I. O., M. Ammerman, and E. Chesnokov, 2009, Estimation of shale's permeability from microseismicity: 78th Annual International Meeting, SEG, Expanded Abstracts, 28, 1581–1585.

Boerner, S. T., B. Bankhead, I. Chaboudy, S. Faruqi, H. Gonzalez, P. Mescher, M. Valderrama, P. Wong, J. Zhou, and E. Mendez. 2004, Jacinto, Paredon, Tepeyil facies and fracture modeling: 73rd Annual Meeting, SEG, Expanded Abstracts, 23, 2773.

Chopra, S. and K. J. Marfurt, 2007, Volumetric curvature attributes adding value to 3D seismic data interpretation: The Leading Edge, **26**, 856–867.

Gardner, G. H. F. and A. Canning, 1994, Effects of irregular sampling on 3D prestack migration: 64th Annual International Meeting, SEG, Expanded Abstracts, 13, 1553–1556.

Gidlow, P. M., G. C. Smith, and P. J. Vail, 1992, Hydrocarbon detection using fluid factor traces, a case study: How useful is AVO analysis?: Joint SEG/EAEG summer research workshop, Technical Program and Abstracts, 78–79.

Gray, D., D. Todorovic-Marinic, and Y. Zheng, 2003, Fractured reservoir characterization using AVAz on the Pinedale anticline: CSEG Recorder, **28**, 40–46.

Gray, D., and D. Todorovic-Marinic, 2004, Fracture detection using 3D azimuthal AVO: CSEG Recorder, **29**, no. 10, 5–8.

Gray, D., and S. Wang, 2009, Towards an optimal workflow for azimuthal AVO: CSEG CSPG, CWLS Joint Convention Abstracts, 111–114.

Hunt, L., S. Hadley, M. Hadley, J. Downton, and B. Durrani, 2008, Interpolation, PSTM, AVO, and a thin gas-charged Viking shoreface in West Central Alberta: CSEG Annual Convention, Convention Abstracts, 177–182.

Khromova, I. and B. Link, 2010, Carbonate fracture case history from Russia and implications for HTD plays in North America: GeoCanada, Convention Abstracts.

Luthi, S. M. and P. Souhaite, 1990, Fracture apertures from electrical borehole scans: Geophysics, **55**, 821–833.

Lynn, H.B., K.M. Simon, and C.R. Bates, 1996, Correlation between P-wave AVOA and S-wave traveltime anisotropy in a naturally fractured gas reservoir: The Leading Edge, **15**, 931–935.

Lynn, H. B., D. Campagna, K. M. Simon, and W. E. Beckham, 1999, Relationship of P-wave seismic attributes, azimuthal anisotropy, and commercial gas pay in 3D P-wave multiazimuth data, Rulison Field, Piceance Basin, Colorado: Geophysics, **64**, 1293–1311.

Maxwell, S. C., C. K. Waltman, N. R. Warpinski, M. J. Mayerhofer, and N. Boroumand, 2009, Imaging seismic deformation induced by hydraulic fracture complexity: SPE Reservoir Evaluation and Engineering, **12**, no. 1, 48–52.

Mazumdar, P., A. Mateeva, and A. Bakulin, 2008, Azimuthal anisotropy characterization with multicomponent virtual shear sources at Rulison Field, Colorado: 78th Annual International Meeting, SEG, Expanded Abstracts, 27, 202–206.

Mosher, C. C., T. Keho, A. Weglein, and D. Foster, 1996, The impact of migration on AVO: Geophysics, **61**, 1603–1615.

Nelson, R., 2001, Geologic analysis of naturally fractured reservoirs: Elsevier.

Roende, H., C. Meeder, J. Allen, S. Peterson, D. Eubanks, and C. Ribeiro, 2008, Estimating subsurface stress direction and intensity from surface full azimuth land data: 78th Annual International Meeting, SEG, Expanded Abstracts, 27, 217–221.

Roth, M. R. and A. Thompson, 2009, Fracture interpretation in the Barnett Shale, using macro and microseismic data: CSEG CSPG, CWLS Joint Convention Abstracts, 497–500.

Rüger, A., 1996, Reflection coefficients and azimuthal AVO analysis in anisotropic media: Ph.D. thesis, Colorado School of Mines.

Sacchi, M. D. and B. Liu, 2005, Minimum weighted norm wavefield reconstruction for AVA imaging: Geophysical Prospecting, **53**, 787–801.

Trad, D., 2007, A strategy for wide-azimuth land data interpolation: 77th Annual International Meeting, SEG, Expanded Abstracts, 26, 946–950.

Trad, D., 2009, Five dimensional interpolation: Five-dimensional interpolation: Recovering from acquisition constraints: Geophysics, **74**, no. 6, V123–V132.

Zheng, Y., S. Gray, S. Cheadle, and P. Anderson, 2001, Factors affecting AVO analysis of prestack migrated gathers: 71st Annual International Meeting, SEG, Expanded Abstracts, 21, 989–992.

Acknowledgments: We thank Dave Gray, (CGGVeritas), Mike Perz (Divestco), Doug Schmitt, Mauricio Sacchi, Mirko Van Der Baan, and Ali Oncel (University of Alberta) for their work on this project. We thank CGGVeritas Data Library Canada and Fairborne Energy Ltd for allowing us to show this information.

Corresponding author: leehunt@telusplanet.net